A miniaturized spin-exchange relaxation-free atomic magnetometer based on uniform light field

Jiajie Li(李佳洁)[1,2], Xiujie Fang(房秀杰)[2,3,†], Renjie Li(李任杰)[1,2], Baodong Chen(陈宝栋)[1,2], Yueyang Zhai(翟跃阳)[1,2], and Ying Liu(刘颖)[1,2,‡]

[1] *Key Laboratory of Ultra-Weak Magnetic Field Measurement Technology (Ministry of Education), School of Instrumentation and Optoelectronic Engineering, Beihang University, Beijing* 100191, *China*
[2] *Zhejiang Provincial Key Laboratory of Ultra-Weak Magnetic-Field Space and Applied Technology, Hangzhou Innovation Institute, Beihang University, Hangzhou* 310051, *China*
[3] *School of Physics, Beihang University, Beijing* 100191, *China*

(Received 31 October 2022; revised manuscript received 21 November 2022; accepted manuscript online 2 December 2022)

We experimentally study the dynamic characteristics of a miniaturized spin-exchange relaxation-free (SERF) magnetometer based on uniform light field. The ceramic ferrule is used to expand the Gaussian beam to improve light intensity uniformity, while the volume of the sensor is also reduced. This scheme makes the magnetometer have better sensitivity when the detected light intensity is less than 3.16 $\mathrm{mW/cm^2}$ at 120 °C. When the temperature rises to 150 °C the sensitivity under the action of uniform light field is 18.5 $\mathrm{fT/Hz^{1/2}}$. The bandwidth of the sensor remains at the original level and meets application needs. The proposed structure improves transverse polarization uniformity within the miniaturized sensor, which is ideal for the magnetoencephalography and magnetocardiography imaging systems.

Keywords: atomic magnetometer, uniform light field, polarization, sensitivity

PACS: 32.10.Dk, 32.80.Qk, 33.35.+r, 07.07.Mp **DOI:** 10.1088/1674-1056/aca7f2

1. Introduction

With the development of optical pumping technology,[1–5] spin-exchange relaxation-free (SERF) atomic magnetometers (AMs) have become a current research hotspot and a kind of mainstream sensors for ultra-sensitive magnetic field detection.[6–8] In just a few years, AMs have surpassed superconducting-quantum-interference-device (SQUID) magnetometers to achieve higher sensitivity in low frequency ranges, and are expected to be further improved to the aT (10^{-18} T) level in the future.[9–11] Traditional SQUID magnetometers are greatly limited in practical applications due to their complex liquid nitrogen refrigeration units and high maintenance costs.[12,13] AMs have the advantages of easy miniaturization, wearable and mobile measurement, and they are widely used in the dynamic measurement of biological magnetoencephalography (MEG), magnetocardiography (MCG), and muscle magnetic field.[14–18]

In general, AMs work on the basis of optically manipulating the coherent precession of polarized atomic spins, to obtain relevant magnetic field information from the dispersion or absorption of the laser beam. The quality of the laser beam is directly related to the sensitivity. In the traditional scheme, a laser passes through the collimating lens and becomes a Gaussian spot with a diameter of 2.7 mm incident the alkali metal vapor. The light intensity in the central area is significantly higher than that in the peripheral area. Due to the characteristics of Gaussian beam and the absorption of resonance laser by atoms, the distribution of pump light intensity in the atomic ensemble is unequal. Fink *et al.* put forward a three-dimensional simulation method of the polarizability.[19,20] Using finite element simulation, the three-dimensional distribution of the polarizability in the alkali metal vapor was obtained, and the effects of aerodynamic effects on the flowing ^{129}Xe gas were researched. Yosuke *et al.* simulated the three-dimensional polarization model of alkali metal atoms of K–Rb mixed pumped magnetometer, and according to the results, it can be seen that the distribution of polarization is not uniform.[21] In the exploration of miniaturized atomic magnetometer, Natsuhiko *et al.* found that the inhomogeneity of pumping spot would saturate the sensitivity of the sensor.[22,23] Therefore, transverse and longitudinal polarizability gradients reduce sensor sensitivity. The uniformity of polarizability is significant for performance of AMs.

The typical method to improve the uniformity of the light field is beam shaping. Current beam shaping methods can be divided into two categories. The first is the aspheric lens method[24] and the birefringent lens group method[25] based on the principles of refraction and transmission in geometric optics. The second is the microlens array method[26] and the liquid crystal spatial light modulator method[27] that use the principle of diffraction. However, in order to improve the spatial resolution, it is necessary to continuously reduce the volume of an AM.[28–31] Miniaturization brings challenges to

†Corresponding author. E-mail: fangxiujie@buaa.edu.cn
‡Corresponding author. E-mail: liu_ying@buaa.edu.cn

© 2023 Chinese Physical Society and IOP Publishing Ltd

sensor light field regulation. A fundamental problem is the limited space for beam shaping, and none of the above methods can be implemented in miniaturized sensors.[32] Taking these factors into consideration, we replace the existing collimator with a ceramic ferrule to emit a diverging light field. The size of the light spot will increase with the propagation distance. Although the enlarged light spot is still in the Gaussian form, the uniformity of the light field will be greatly improved. Through measurement, it is found that when the beam reaches the vapor cell, the spot expands to about 4 mm, meeting the application requirements. Compared the performance of the AM under the uniform light field with that under the traditional collimated light beam, it can be found that the uniform beam can make the magnetometer maintain good sensitivity at high temperatures. When the PD detection light intensity is low, this scheme is proven to improve the performance of the sensor. At the same time, the bandwidth of the miniaturized sensor is also adequate the application requirements.

2. Theoretical method

The optical pumping rate $R_{\rm op}$, representing the average rate at which unpolarized atoms absorb photons from the pump beam, is directly related to the light intensity. $R_{\rm op}$ can be expressed as $R_{\rm op} = aI(z)$, where z denotes the position in the atomic ensemble and a is the pump rate per unit laser intensity.[33,34] The electron spin polarization along the pumping direction is defined as $P_z = R_{\rm op}/(R_{\rm op}+R_{\rm sd})$, where $R_{\rm sd}$ is the rate of spin destruction from collisions with other atoms.[35] Therefore, we can obtain the relationship between the spin polarization and the laser intensity as

$$P_z = \frac{I(z)}{I(z)+1/A}, \tag{1}$$

where $a/R_{\rm sd}$ is replaced with A. Due to the absorption of circularly polarized light by rubidium atoms, the attenuation of light intensity in the cell with propagation distance can be expressed as[37]

$$I(z) = \frac{1}{A}W(AI(0)\exp(AI(0)-n\sigma(v)z)), \tag{2}$$

where $W(z)$ is the Lambert W-function and $W(z)\,{\rm e}^{W(z)} = z$,[36] n is the density of rubidium atoms, and $\sigma(v)$ is the absorption cross section determined by the laser frequency v. We calculate the polarization distribution of electrons, and the normalized results of the transverse section at $z = -1.5$ mm and the longitudinal section at $y = 0$ mm are shown in Fig. 1. It can be found that the uniformity of electron polarization based on uniform light field is higher. Uniform light field can effectively reduce the polarization gradient caused by Gaussian beam.

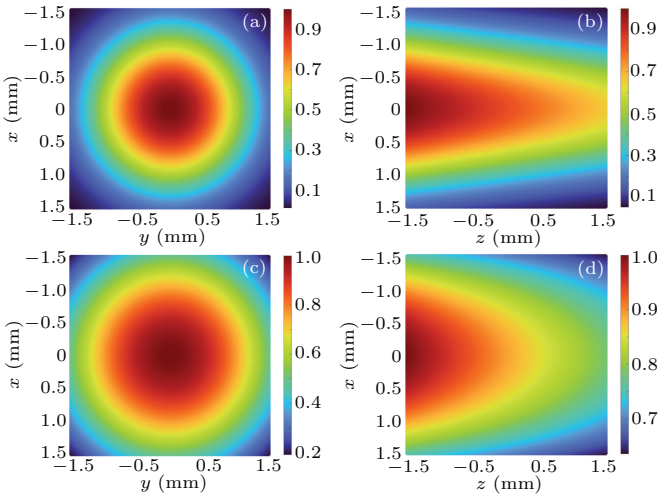


Fig. 1. Normalized electron polarizability simulation results: (a) collimated light, spot diameter 1.35 mm, transverse; (b) collimated light, spot diameter 1.35 mm, longitudinal; (c) uniform beam, transverse; (d) uniform beam, longitudinal.

In the presence of spin exchange, the evolution of the density matrix most accurately describes the behavior of atomic spins. However, in the SERF region where the atomic spin exchange rate is significantly higher than the Larmor precession frequency, the polarization evolution of electron spins can be expressed by the Bloch equation[38]

$$\frac{{\rm d}\boldsymbol{P}}{{\rm d}t} = D\nabla^2\boldsymbol{P} + \frac{1}{q}\left[\gamma_{\rm e}\boldsymbol{B}\times\boldsymbol{P} - R_{\rm rel}\boldsymbol{P} + R_{\rm op}\left(\frac{1}{2}\boldsymbol{s}-\boldsymbol{P}\right)\right], \tag{3}$$

where $\boldsymbol{P} = (P_x, P_y, P_z)$ is the electron spin polarization, D is the diffusion coefficient, q is the nuclear slowing-down factor ranging, $\gamma_{\rm e}$ is the electron's gyromagnetic ratio, $R_{\rm rel}$ is the spin-relaxation rate, and $s = +1$ is the photon spin vector of the $+\sigma$ pump beam. Since the high pressure buffer gas suppresses the diffusion of atoms, we usually ignore the first term on the right side of Eq. (3). The second term on the right represents the Larmor precession of alkali metal atoms. The third term describes the depolarization effect of the spin relaxation, and the last term is the effect of optical pumping on atomic spin.

To suppress the influence of low-frequency noise, transverse magnetic field modulation is adopted. We firstly zero out the magnetic field components in the x, y, and z directions. Then apply modulation field $B_1\cos(\omega t)$ and calibration field $B_{\rm mod}\cos(\omega_{\rm mod}t)$ in x direction. Therefore, the magnetic field component in the x direction is expressed as $B_x = B_0 + B_1\cos(\omega t) + B_{\rm mod}\cos(\omega_{\rm mod}t)$, where B_0 is the static field. We demodulate the first harmonic component of the phase-locked amplifier, and the output of the magnetometer can be obtained as

$$\partial P_z = \frac{2R_{\rm op}J_0(u)J_1(u)}{(R_{\rm op}+R_{\rm rel})^2 + (\gamma_{\rm e}B_{x0})^2}\gamma_{\rm e}\partial B_{x0}, \tag{4}$$

where $J_n(u)$ is a Bessel function of the first kind of the order n, and $u = \gamma_{\rm e}B_1/q\omega$. According to the above formula, the output signal of the AM is in the form of a dispersion curve with B_{x0} as the variable.

The sensitivity can be defined by the following formula:

$$\partial B = \frac{\Delta B}{(S/N)}, \tag{5}$$

where ΔB is the linewidth, and (S/N) is the signal-to-noise ratio

$$(S/N) \propto k\sqrt{I(0)\,\mathrm{e}^{-l_{\mathrm{OD}}} l_{\mathrm{OD}}\,\mathrm{e}^{l_{\mathrm{OD}}P_0\left(1-\frac{q^2u^2}{2}\right)} P_0 q u \gamma_e B_1 \frac{\tau}{\tau^2\omega^2+1}}, \tag{6}$$

where k is the calibration factor,[39] P_0 is polarizability under normal operation, τ is transverse spin relaxation time, and $l_{\mathrm{OD}} = n\sigma(v)z$ is the optical depth with n being the density of the alkali vapor and $\sigma(v)$ the absorption cross section as a function of the laser frequency. It can be seen from Eq. (6) that the signal-to-noise ratio is positively correlated with $I(0)$.

3. Experimental setup

The internal structure of the AM is shown in Fig. 2. The glass cell is made of borosilicate glass with an outer diameter of 4 mm and an inner diameter of 3 mm. The vapor cell contains a small drop of isotopically enriched ^{87}Rb and N_2, and the pressure broadening is 11 GHz. Nitrogen acts as an inert gas that can restrain the diffusion of rubidium atoms and inhibit the collision rate of the wall, and also acts as a quenching gas to reduce radiation trapping. To minimize magnetic noise from heating, a high-frequency alternating current of 200 kHz is used to heat the cell. A non-magnetic PT1000 is used to measure temperature signal in real time, and the temperature fluctuation of the magnetometer is less than 50 mK when it works at 120 °C. At this temperature, rubidium atoms can reach a density of 10^{13} cm^{-3} and operate in the SERF state. The vapor cell is surrounded by a triaxial coil to null the DC magnetic field within the magnetic shields and generate the modulation field. For the compact internal structure, the electrical signals of the sensors are transmitted by a flexible printed circuit board (FPCB). A distributed feedback (DFB) laser (795 nm, UniQuanta) emits linear polarization light. The light is introduced into the sensor through a polarization-maintaining fiber (PMF). The divergent beam emitted from the standard ceramic ferrule is not collimated by a collimating lens. After passing through a reflecting prism, a linear polarizer and a quarter wave plate, the beam enters the vapor cell in the circularly polarized state. Different from the two-beam scheme, the single-beam scheme uses a circularly polarized light for pumping and probing. We generally obtain the best signal-to-noise ratio by optimizing the optical power and wavelength.

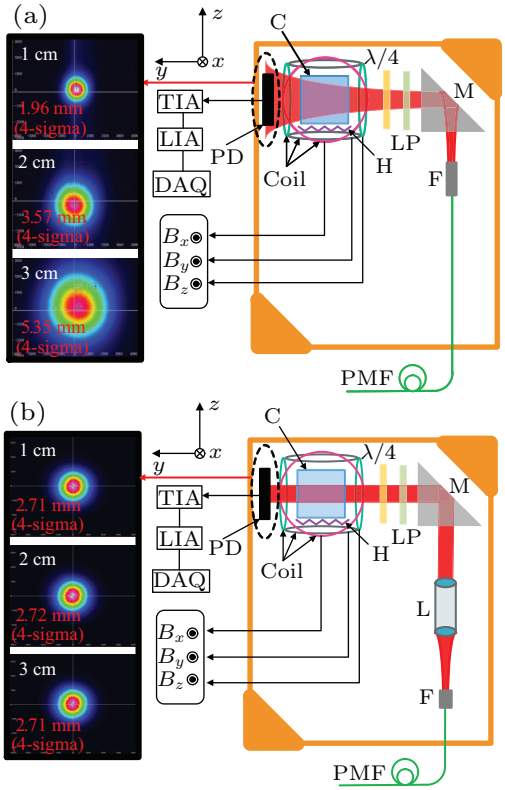


Fig. 2. Schematic diagram of the optical path and electrical signal transmission inside the AM. (a) Uniform light field. The variation of the spot size with the exit distance is shown on the left, in which the white font represents the exit distance and the red font records the lateral size. (b) Collimated light field. F: fiber port; L: collimating lens; M: reflecting prism; LP: linear polarizer; $\lambda/4$: quarter wave plate; H: heating film; C: rubidium vapor cell; PD: photodetector; TIA: transimpedance amplifier; LIA: lock-in amplifier; DAQ: data acquisition.

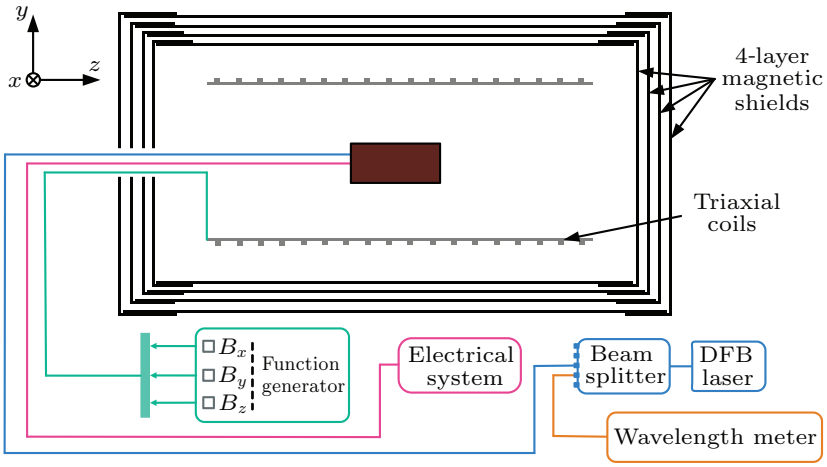


Fig. 3. Experimental setup for AM testing. The blue line connected to AM denotes the polarization-maintaining fiber (PMF) that transmits the laser, and the pink line represents the flexible printed circuit board (FPCB) that conducts the electrical signals.

Figure 3 is the schematic diagram of the experimental test system. The magnetic shielding system consists of three-layers cylindrical μ-metal shield and the outermost co-axial aluminum layer. The quasi-static shielding factor is 10^5, and the geomagnetic field can be attenuated to several nT after degaussing. The AM is placed in the middle of the magnetic shielding barrel to obtain the desired magnetic shielding effect. The triaxial coils generate calibration magnetic field.

4. Results and discussion

We use collimating light field and uniform light field to test atomic magnetometer when PD senses different light intensity. The light intensity was gradually increased from 1.05 mW/cm^2 to 8.42 mW/cm^2, and the dispersion curves were obtained by applying different voltages to the x-axis coil. The test results are shown in Fig. 4.

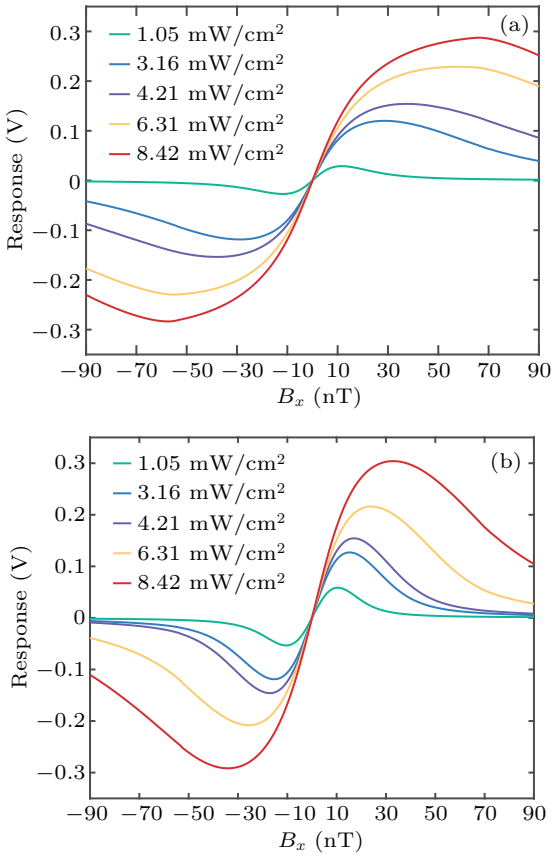


Fig. 4. Dispersion curve at different light intensities: (a) uniform light field, (b) collimated light field.

The amplitude of the AM response signal increases with the rise of the input light intensity within this range. As the applied magnetic field on the x-axis goes up, a peak appears in the response signal. When the light intensity measured by PD is consistent, the linewidth measured by uniform light field is obviously larger than that measured by collimated light field. According to $\Delta B = (R_{\rm op} + R_{\rm rel})/\gamma_{\rm e}$, the linewidth is determined by the pumping rate and relaxation rate. All operations are carried out by using the same vapor cell, and the conditions other than pumping beam remain as same as possible. We let $R_{\rm rel1}$ and $R_{\rm op1}$ denote the relaxation rate and pumping rate operating under a uniform light field, while $R_{\rm rel2}$ and $R_{\rm op2}$ are that operating under a collimated light field. Assume that $R_{\rm rel1} = R_{\rm rel2}$, so $R_{\rm op1} > R_{\rm op2}$. The actual output light intensity of the uniform beam is greater than the detection value of PD, and the uniform spot area is larger than the sensitive area of PD.

A calibration magnetic field of 30.5 Hz is applied on the x-axis, and the AM output time-domain signal is FFT transformed to obtain the sensitivity test curve. The sensitivities under different PD detection light intensity are compared, and the experimental results are shown in Fig. 5 and Table 1.

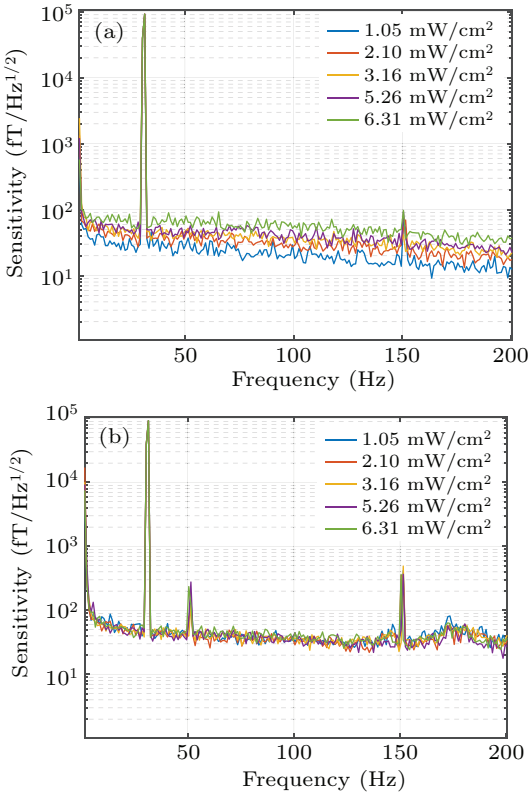


Fig. 5. Sensitivity comparison at different light intensities: (a) uniform light field, (b) collimated light field.

Table 1. Sensitivity data at different light intensities.

Light intensity (mW/cm^2)	Uniform beam sensitivity (fT/Hz$^{1/2}$)	Collimated beam sensitivity (fT/Hz$^{1/2}$)
1.05	22.52	36.42
2.10	27.18	37.85
3.16	36.80	38.50
5.26	39.22	33.13
6.31	51.31	37.62

When the light intensity is less than 3.16 mW/cm^2, the sensitivity optimized for at least 10 fT/Hz$^{1/2}$. When the PD detection value is similar, the incident light in Fig. 5(a) is more uniform and more intense in the cross section. It can be seen from Eq. (6) that (S/N) of Fig. 5(a) is also improved. For the sensor operating with the uniform light field, despite the larger linewidth ΔB, the sensitivity will be better due to the greatly improved signal-to-noise ratio, when the light intensity is less

than 3.16 mW/cm^2. With the further increase of the incident light intensity, photon shot noise and technical noise will augment, resulting in poor sensitivity.

We fixed the initial incident light intensity and conducted comparative tests at different temperatures. The experimental results are shown in Fig. 6 and Table 2 in the range of 120–150°C. When the temperature is higher than 140 °C the magnetometer based on the collimated light field has a very weak PD detection signal due to the large light absorption, and the signal ratio is very poor. However, the magnetometer based on a uniform light field has a larger response signal due to the more uniform polarizability and the stronger light intensity felt by the atoms in the cell. Although the PD detection light intensity is the same, the signal-to-noise ratio is higher and the sensitivity is fabulous.

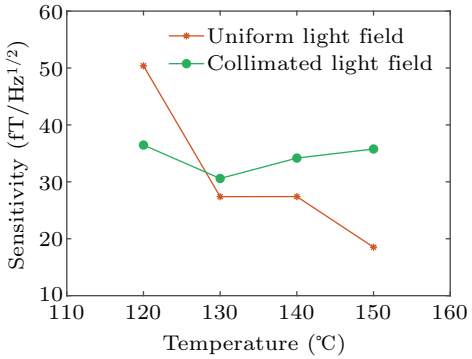


Fig. 6. Sensitivity comparison at different temperatures.

Table 2. Sensitivity data at different temperatures.

Temperature (°)	Uniform beam sensitivity (fT/Hz$^{1/2}$)	Collimated beam sensitivity (fT/Hz$^{1/2}$)
120	50.39	36.46
130	27.39	30.59
140	27.41	34.17
150	18.51	35.77

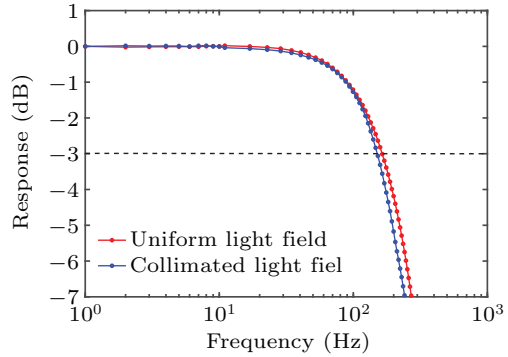


Fig. 7. Normalized frequency response of AM.

Sweep the AM signal at different frequencies, and the function curve of the response with the frequency is shown in Fig. 7. The sensor bandwidth based on a uniform light field is 164.1 Hz, while the bandwidth of the conventional structure is 150.8 Hz. It shows that the structure can perform weak magnetic measurement in the original frequency band, and meets the current application requirements.

5. Conclusion

In summary, we have demonstrated a method to improve the lateral uniformity of the light field within a miniaturized AM. The size of the AM has been further reduced by removing the collimating lens. We perform a three-dimensional simulation of the electron polarizability distribution and find that the polarizability lateral gradient is suppressed. Through the comparison experiment with the traditional Gaussian collimated light field, we find that when the light intensity is less than 3.16 mW/cm^2, the AM has higher signal-to-noise ratio, and the sensitivity is optimized by about 30% on average. Moreover, the sensor has better performance under the working environment of 130 ℃–150 ℃. The sensitivity reaches 18.5 fT/Hz$^{1/2}$ at 150 ℃. Further refinements of this structure are possible. The propagation distance of the laser before entering the cell can be adjusted to find better working conditions. The miniaturized AM structure proposed in this paper is especially suitable for array MEG and MCG applications, and has broad application prospects.

Acknowledgement

Project supported by the National Natural Science Foundation of China (Grant No. 62003020).

References

[1] Lü X Y, Zhu R B, Song H, Su N and Chen G 2019 *Acta Phys. Sin.* **68** 214201 (in Chinese)
[2] Wang X, Zou Y, He Z, Liu G and Ma X 2020 *Chin. Phys. B* **29** 084208
[3] Zhai Y, Carson C H, Henderson V A, Griffin P F, Riis E and Arnold A S 2018 *Optica* **5** 805
[4] Qiu X, Xu Z, Peng X, Li L, Zhou Y, Wei M, Z M and Xu X 2020 *Appl. Phys. Lett.* **116** 034001
[5] Liu J, Savici A T, Granroth G E, Habicht K, Qiu Y, Hu J, Mao Z and Bao W 2018 *Chin. Phys. Lett.* **35** 127401
[6] Zhang Y, Tian Y, Li S, Chen J and Gu S 2019 *Phys. Rev. Appl.* **12** 011004
[7] Brazhnikov D, Ignatovich S, Mesenzova I, Novokreshchenov A and Goncharov A 2020 *Opt. Lett.* **45** 3309
[8] Fang J C, Wang T, Zhang H, Li Y and Cai H W 2015 *Chin. Phys. B* **24** 060702
[9] Kominis I K, Kornack T W, Allred J C and Romalis M V 2003 *Nature* **422** 596
[10] Tang F and Zhao N 2020 *Chin. Phys. B* **29** 090303
[11] Allred J, Lyman R N, Kornack T W and Romalis M V 2002 *Appl. Phys. Lett.* **89** 130801
[12] Pan Y P, Wang Y, Yang R T, Tang Y, Liu X Y, Jin H, Ma L, Lin Y, Wang Z, Ren J, Wang Y and Chen L 2020 *Chin. Phys. Lett.* **37** 080702
[13] Okada Y, Hnen M, Pratt K, Mascarenas A, Miller P, Han M, Robles J, Cavallini A, Power B, Sieng K, Sun L M, Lew S, Doshi C, Ahtam B, Dinh C, Esch L, Grant E, Nummenmaa A, Paulson D and Paulson D 2016 *Rev. Sci. Instrum.* **87** 094301
[14] Hill R M, Devasagayam J, Holmes N, Boto E, Shah V, Osborne J, Safar K, Worcester F, Mariani C, Dawson E, Woolger D, Bowtell R, Taylor M J and Brookes M J 2022 *NeuroImage* **253** 119084

[15] Tang J, Zhai Y, Cao L, Zhang Y, Li L, Zhao B, Zhou B, Han B and Liu G 2021 *Opt. Express* **29** 15641

[16] Elzenheimer E, Laufs H, Schulte-Mattler W and Schmidt G 2020 *IEEE Trans. Neural Syst. Rehabil. Eng.* **22** 1018

[17] Borna A, Iivanainen J, Carter T R, McKay J, Taulu S, Stephen J and Schwindt P D 2022 *NeuroImage* **247** 118818

[18] Strand S, Lutter W, Strasburger J F, Shah V, Baffa O and Wakai R T 2019 *J. Am. Heart Assoc.* **8** e013436

[19] Fink A, Baumer D and Brunner E 2005 *Phys. Rev. Appl.* **72** 053411

[20] Fink A and Brunner E 2007 *Appl. Phys. B: Lasers Opt.* **89** 65

[21] Ito Y, Sato D, Kamada K and Kobayashi T 2016 *Opt. Express* **24** 15391

[22] Ito S, Ito Y and Kobayashi T 2019 *Opt. Express* **27** 8037

[23] Mizutani N, Okano K, Ban K, Ichihara S, Terao A and Kobayashi T 2014 *AIP Adv.* **4** 057132

[24] Lin H F, Jan H T, Chen C F and Hsu H C 2010 *Optik* **121** 2250

[25] Sinchuk K, Dudley R, Graham J D, Clare M, Woldeyohannes M, Schenk J O, Ingel R P, Yang W G and Fiddy M A 2010 *Opt. Express* **18** 463

[26] Zhong K, Gao Y, Li F, Zhang Z and Luo N 2014 *Optik* **125** 2413

[27] Chen X, Fang X, Ma D, Liu Y, Cao L and Zhai Y 2022 *Appl. Opt.* **61** C55

[28] Shah V K and Wakai R T 2013 *Phys. Med. Biol.* **58** 8153

[29] Sulai I A, DeLand Z J, Bulatowicz M D, Wahl C P, Wakai R T and Walker T G 2019 *Rev. Sci. Instrum.* **90** 085003

[30] Colombo A P, Carter T R, Borna A, Jau Y Y, Johnson C N, Dagel A L and Schwindt P D 2016 *Opt. Express* **24** 15403

[31] Hill R M, Boto E, Holmes N, Hartley C, Seedat Z A, Leggett J, Roberts G, Shah V, Tierney T M, Woolrich M W, Stagg C J, Barnes G R, Bowtell R, Slater R and Brookes M J 2019 *Nat. Commun.* **10** 4785

[32] Yuchen J, Zhanchao L, Binquan Z, Xiaoyang L, Wenfeng W, Jinpeng P, Ming D, Yueyang Z and Jiancheng F 2019 *J. Phys. D: Appl. Phys.* **52** 355001

[33] Lancor B, Babcock E, Wyllie R and Walker T G 2010 *Phys. Rev. Appl.* **82** 043435

[34] Appelt S, Baranga A B A, Erickson C J, Romalis M V, Young A R and Happer W 1998 *Phys. Rev. A* **58** 1412

[35] Seltzer S J 2008 *Developments in alkali-metal atomic magnetometry* (Ph.D. Dissertation) (Princeton University)

[36] Hwang C and Cheng Y C 2005 *Automatica* **41** 1979

[37] Li R, Quan W and Fang J 2017 *IEEE Photon. J.* **9** 1

[38] Ledbetter M P, Savukov I M, Acosta V M, Budker D and Romalis M V 2008 *Phys. Rev. A* **77** 033408

[39] Wang Y, Jin G, Tang J, Zhou W, Han B, Zhou B and Shi T 2022 *Opt. Express* **30** 23587